2009

A Novel Technology for the Imaging of Acidic Prostate Tumors by Positron Emission Tomography

Amy L. Vāvere

Gráinne B. Biddlecombe

See next page for additional authors

Citation/Publisher Attribution

Vāvere, A. L., Biddlecombe, G. B., Spees, W. M., Garbow, J. R., Wijesinghe, D., Andreev, O. A., Engelman, D. M.,...Lewis, J. S. (2009). A Novel Technology for the Imaging of Acidic Prostate Tumors by Positron Emission Tomography. *Cancer Res., 69*(10), 4510-4516. doi: 10.1158/0008-5472.CAN-08-3781
Available at: http://dx.doi.org/10.1158/0008-5472.CAN-08-3781

Published in final edited form as:
Cancer Res. 2009 May 15; 69(10): 4510–4516. doi:10.1158/0008-5472.CAN-08-3781.

A Novel Technology for the Imaging of Acidic Prostate Tumors by Positron Emission Tomography

Amy L. V vere[1], **Gráinne B. Biddlecombe**[1], **William M. Spees**[2], **Joel R. Garbow**[2], **Dayanjali Wijesinghe**[3], **Oleg A. Andreev**[3], **Donald M. Engelman**[4], **Yana K. Reshetnyak**[3], and **Jason S. Lewis**[1,5]

1 *Division of Radiological Sciences, Washington University School of Medicine, St. Louis, MO, 63110, USA*

2 *Biomedical MR Laboratory Department of Radiology, Washington University School of Medicine, St. Louis, MO, 63110, USA*

3 *Physics Department, University of Rhode Island, Kingston, RI, 02881*

4 *Department of Molecular Biophysics and Biochemistry, Yale University, New Haven, CT, 06520*

5 *Department of Radiology, Memorial Sloan-Kettering Cancer Center, New York, NY, 10065, USA*

Abstract

Solid tumors often develop an acidic environment due to the Warburg Effect. The effectiveness of diagnosis and therapy may therefore be enhanced by the design and use of pH-sensitive agents that target acidic tumors. Recently, a novel technology was introduced to target acidic tumors using pHLIP (pH Low Insertion Peptide), a peptide that inserts across cell membranes as an α-helix when the extracellular pH is acidic. In this study we expanded the application of the pHLIP technology to include positron emission tomography (PET) imaging of the acidic environment in prostate tumors using ^{64}Cu conjugated to the pHLIP peptide (^{64}Cu-DOTA-pHLIP). Studies demonstrated that this construct avidly accumulated in LNCaP and PC-3 tumors, with higher uptake and retention in the LNCaP tumors. Uptake correlated with differences in the bulk extracellular pH (pH_e) of PC-3 and LNCaP tumors measured in MR spectroscopy experiments by the ^{31}P chemical shift of the extracellular pH marker 3-aminopropylphosphonate. This manuscript introduces a novel class of non-invasive pH-selective PET imaging agents and opens new research directions in the diagnosis of acidic solid tumors.

Keywords

extracellular pH; PET; pHLIP; Cu-64

Introduction

Studies of the gene signatures of cancer cells indicate that many different genes are either up- or down-regulated, even within a given type of tumor, so it is problematic to rely on any single biomarker for the diagnosis of even a single type of cancer (1). However, physiological processes (e.g., hypoxia and acidity), which are present in 90% of tumor microenvironments, are considered promising environmental markers for tumor targeting (2,3). In particular, an

Corresponding Author: Jason S. Lewis, Ph.D., Department of Radiology, Memorial Sloan-Kettering Cancer Center, 1275 York Avenue, New York, New York 10065, Tel: (646) 888-3038, Fax: (646) 422 0408, E-mail: E-mail: lewisj2@mskcc.org.
Current address: Amy L. Vāvere PhD, St. Jude Children's Research Hospital, Memphis, TN, 38105, USA

acidic tumor environment plays a significant role in tumor progression and is often associated with increased invasion and metastasis (4–6) as well as resistance to drug therapies (5,7,8). Recently, a correlation was observed between extracellular pH (pH_e) and overall survival following treatment with combined hyperthermia and radiation therapy for spontaneous sarcomas in canines (9). Tumor pH has practical importance because most anticancer drugs must be transported either by active transport or by passive diffusion into cells, where they frequently undergo further metabolism. As all of these processes might be pH sensitive, the cytotoxic activity of an anticancer drug could depend on both the intracellular pH (pH_i) and the pH_e. In the case of chemotherapeutic agents that are weak acids or bases and enter targeted cells *via* passive diffusion, it is the non-ionized form that crosses the cell membrane. It also has been suggested that modulation of tumor pH, both pH_i and pH_e, could be used to increase the uptake of therapeutic drugs (7,10–12). Delineation of pH_i from pH_e is impossible with electrode-based techniques due to the scale of the electrode compared to the tissue. Thus, non-invasive tools for monitoring pH_e and the effectiveness of its modulation could be extremely valuable.

A number of MR-based methods for the estimation of pH_e in animal tumor models have been introduced in recent years. These approaches include use of T_1-weighted MRI with extracellular contrast agents that exhibit pH-dependent ^1H relaxation enhancement (13), ^1H and ^{31}P pH-dependent chemical shift measurements of exogenous extracellular species (14–16), and ^{13}C chemical shift imaging of hyperpolarized ^{13}C-labeled bicarbonate (17). Studies with the ^{31}P extracellular pH indicator 3-aminopropylphosphonate (3-APP) have confirmed that the average pH_e of tumors is acidic, with values reaching as low as 6.0 (18). At present, however, these techniques cannot be readily translated to the clinic.

Positron emission tomography (PET) is a widely used molecular imaging modality both in clinical and research settings (19). The use of ^{64}Cu as a PET nuclide, and the basis for new radiopharmaceuticals, is particularly attractive given its 12.74 h half life (20). ^{64}Cu-complexes have been studied as PET agents with the nuclide incorporated into either small molecules or peptides (21,22). Here we present the ^{64}Cu PET imaging of prostate tumors using the recently discovered acid-targeting peptide – pHLIP (pH Low Insertion Peptide) (23–25). The pHLIP peptide contains 37 residues. At neutral extracellular pH, it interacts with the surface of membranes as an unstructured peptide, but at acidic pH_e (<7.0) it inserts across the membrane and forms a stable transmembrane α-helix (24). We have shown that pHLIP can target a variety of fluorescent dyes conjugated to its N-terminus to a tissue with elevated extracellular acidity *in vivo*, and also that it can deliver chemotherapeutics into cells through interactions with the membrane lipid bilayer, avoiding the need for any specific interaction with membrane proteins (23,25,26). The present study was undertaken to evaluate whether it is possible to delineate lower pH_e in prostate tumors *in vivo* with 64Cu conjugated to the pHLIP peptide (^{64}Cu-DOTA-pHLIP), the first compound of a new generation of novel pH-selective tumor PET imaging agents.

Materials and Methods

All chemicals, unless otherwise stated, were purchased from Sigma-Aldrich Chemical Company, Inc (St. Louis, MO). Radioactive samples were counted in a radioisotope calibrator (Capintec, Inc., Ramsey, NJ) for determination of mCi and an automated-well Beckman 8000 gamma counter (Beckman Coulter, Fullerton, CA) for counts per minute. Male athymic nu/nu mice were purchased from the National Cancer Institute (Frederick, MD). Human prostate carcinoma tumor cell lines PC-3 and LNCaP were obtained from American Type Culture Collection (Manassas, VA) and maintained by serial passage in cell culture.

Preparation of peptides and ^{64}Cu radiolabeling

All peptides were prepared by solid-phase peptide synthesis using standard Fmoc (9-fluorenylmethyloxycarbonyl) chemistry and purified by reverse phase chromatography (on a C18 column) at the W. M. Keck Foundation Biotechnology Resource Laboratory at Yale University. Peptide sequences were:
ACEQNPIYWARYA**D**WLFTTPLLLL**D**LALLVDADEGTG (pHLIP) and,
ACEQNPIYWARYA**K**WLFTTPLLLL**K**LALLVDADEGTG (K-pHLIP). The N-terminus of the pHLIP peptide was covalently conjugated to 1,4,7,10-tetraazacyclododecane-1,4,7-tris-acetic acid-10-maleimidoethylacetamide, a maleimide-containing derivative of DOTA - a chelator used for the effective binding of copper radionuclides (27). The peptides were incubated with 2X molar excess of DOTA-maleimide (Macrocyclics Inc.) in the presence of 2 mM EDTA in PBS buffer pH 7.4 overnight, at 4°C. Free DOTA-maleimide and EDTA were removed by a Sephadex G-10 spin column equilibrated with PBS buffer, pH 7.4. The concentration of peptide was determined by absorbance at 280 nm using a molar extinction coefficient of ε_{280}=13,940 $M^{-1}cm^{-1}$. The composition and degree of conjugation were confirmed by mass spectrometry and HPLC. The peptides were analyzed by electrospray mass spectrometry (ES+) (DOTA-pHLIP: *m/z* calcd for $C_{215}H_{323}N_{50}O_{66}S$ (M^+) = 4693.3, found 1174.74 ($M+4H^+$) and 1565.4 ($M+3H^+$)). Reversed phase HPLC involved a Waters X-Bridge (C4, 4.6 × 75 mm) column with a gradient (0 – 2 min 20%B to 40%B; 2 – 7 min 40%B to 70% B; 7 – 10 min 70%B to 100%B (solvent A: 0.01% TFA in water; solvent B: 0.01% TFA in acetonitrile) at a flow rate of 1 mL/min. Detection was accomplished at 280 nm and the retention times for DOTA-pHLIP and DOTA-K-pHLIP were 5.45 and 4.82 min, respectively. The peptides were stored at −80°C.

^{64}Cu was produced at Washington University School of Medicine and processed by previously reported literature methods (28). Maximal labeling for both constructs was achieved in 0.5 M ammonium acetate buffer pH 5.5 at 25°C for 30 minutes at a ratio of 1:1 (μg:mCi). Prior to purification, 5 mM of EDTA was added to scavenge any uncomplexed ^{64}Cu. Purification was achieved by C18 SepPak Light using 100% ethanol as the eluent. Purity and labeling efficiency were determined by radio-TLC on silica using 10% ammonium acetate:methanol (50:50).

Acute biodistribution

All animal experiments were performed in compliance with the Guidelines for the Care and Use of Research Animals established by Washington University's Animal Studies Committee. 20–25 g male athymic mice (NCI) were implanted in the right flank with either 1×10^7 PC-3 or LNCaP human prostate adenocarcinoma cells in 100 μL cell media with >90% viability. The LNCaP cells were implanted using Matrigel (BD Biosciences, San Jose, CA). Tumors were allowed to grow to approximately 0.5 – 0.75 cm^3 in volume. Mice were randomized prior to the study. To investigate specific uptake of tumor, organ, and other non-target tissues, a small amount of ^{64}Cu-DOTA-pHLIP (~28 μCi, 0.22 μg) was injected intravenously into each of the mice bearing palpable PC-3 or LNCaP tumors. The animals were sacrificed at selected time points after injection (1, 4, 24, and 48 hours; n = 4–5) and desired tissues were removed, weighed, and counted for radioactivity accumulation. The percentage injected dose per gram (%ID/g) and percentage injected dose per organ (%ID/organ) were calculated by comparison to a weighed, counted standard solution. An additional group of PC-3 mice were injected with ^{64}Cu-DOTA-K-pHLIP (~28 μCi, 0.22 μg) and were sacrificed at 1 h (n = 5). Due to a technical error an additional group of mice were injected and just the kidneys were removed. Since the aspartic acid residues have been changed to lysines in the transmembrane portion, the K-pHLIP peptide should not have the ability to form an α-helix and span the membrane of the cells in acidic environments. On a different day, an additional cohort of LNCaP-bearing mice (which were implanted with a different passage of LNCaP cells, n = 8) were split into two groups, with the first group receiving 150 mM bicarbonated water at pH 8.0 (3.1455 g of

sodium bicarbonate, dissolved in 250 mL drinking water) *ad libitum* for 7 days prior to the acute biodistribution study (4 h) to modulate tumor pH_e (12,25,29) and the second group receiving regular drinking water. MRS studies were performed on the tumors in all of these mice prior to biodistribution.

Small Animal PET

Imaging ^{64}Cu-DOTA-pHLIP was performed on two tumor models using a microPET-F220 (30). Imaging was performed in 10-minute static sessions, with a collection of 600 frames per session. Isoflurane (2%) was used as an inhaled anesthetic to induce and maintain anesthesia during imaging. Male athymic mice implanted in the right flank with PC-3 (n = 4) or LNCaP (n = 10) human prostate adenocarcinoma cells which were allowed to grow until palpable. At this point, the mice were injected IV with 200 μCi ^{64}Cu-DOTA-pHLIP and were then imaged in pairs at 1, 4, and 24 hours post injection. Images were reconstructed by Fourier rebinning followed by two-dimensional Ordered Subset Expectation Maximization (OSEM). Small animal PET images were evaluated by analysis of the standardized uptake value (SUV) of the tumor and muscle using the software ASIPRO (Concorde MicroSystems, Inc.). The average radioactivity concentration within the tumor or tissue was obtained from the average pixel values reported in nCi/cc within a volume of interest (VOI) drawn around the entire tumor or tissue on multiple, consecutive transaxial image slices. SUVs were calculated by dividing this value, the decay-corrected activity per unit volume of tissue (nCi/mL), by the injected activity per unit of body weight (nCi/g).

Magnetic Resonance Spectroscopy

In vivo extracellular pH_e was determined in LNCaP and PC3 tumors within the 24-hour period immediately prior to injection of ^{64}Cu-labeled pHLIP peptides. Non-invasive measurements of pH_e were based on the ^{31}P MR-observable chemical shift of 3-aminopropylphosphonate (3-APP) (31). Prior to MR measurements, mice bearing PC-3 (n = 3) or LNCaP (n = 6) tumors were anesthetized with isoflurane and were maintained on isoflurane/O_2 (1.25 % v/v) throughout data collection. Each anesthetized mouse received an i.p. injection of 0.35 mL of 3-APP (Sigma-Aldrich, St. Louis, MO) solution prepared at a concentration of 75 mg 3-APP/mL in isotonic saline. After injection, mice were placed in a head holder with a nose cone for delivery of anesthetic gas and a custom-built ^{31}P MR surface coil was placed around the tumor.

^{31}P MR studies were performed using a small-animal MR scanner based on a Magnex Scientific Instruments (Oxford, UK) 11.74 tesla (^{31}P resonance frequency 202.3 MHz), 26-cm horizontal-bore magnet interfaced with a Varian NMR Systems (Palo Alto, CA) INOVA console. Magnetic field homogeneity was optimized by shimming on the free induction decay of the tumor water resonance, observed through the ^{31}P MR surface coil. ^{31}P spectral acquisition parameters were: sweep width of 20,000 Hz, 0.3 s acquisition time, 4.06 s repetition time and a 60° excitation pulse. A total of 512 transients were averaged for each measurement; thus, the total length of each ^{31}P scan was 34 minutes. MR data were processed with a matched filter (30 Hz line-broadening) and frequency estimates for the ^{31}P MR spectral components were performed using a Bayesian Probability Theory analysis package developed at Washington University (32). The resulting estimated chemical-shift difference between 3-APP and the pH-independent α-nucleoside triphosphate (α-NTP) resonance (33) was used to determine extracellular pH based on the fitting parameters provided by Gillies, *et al* (31).

Statistics

Statistically significant differences between mean values were determined using analysis of variance (ANOVA) coupled to Scheffe's test or, for statistical classification, a Student's t-test was performed. Differences at the 95% confidence level ($P < 0.05$) were considered significant.

Results

^{64}Cu-DOTA-pHLIP and ^{64}Cu-DOTA-K-pHLIP can be obtained in high yield and good specific activity

^{64}Cu labeling of DOTA-pHLIP was attempted at various pH values between 4.5 and 9.2 using 0.125–0.2 M ammonium acetate. Optimal labeling was achieved in 0.5 M ammonium acetate buffer pH 5.5 at 25°C for 30 minutes at a ratio of 1:1 (μg:mCi) at a specific activity of 1591 mCi/μmol. Without heating, the labeled solution remained stable overnight. Radiochemical purity was consistently >95% following EDTA scavenge and SepPak purification, as shown by radio-TLC on silica using 10% ammonium acetate:methanol (50:50). As a control, we used a mutant version of pHLIP (K-pHLIP) in which key Asp residues of the transmembrane part of pHLIP were replaced by positively charged Lys residues (Figure 1). These changes prevent the peptide from inserting across the cell membrane and forming an α-helix at acidic pH.(25) The mutant/control peptide (K-pHLIP) was labeled in a similar manner at a specific activity of 1713 mCi/μmol at >95% radiochemical purity.

Acute biodistribution of ^{64}Cu-DOTA-pHLIP in PC3 and LNCaP, and ^{64}Cu-DOTA-K-pHLIP in PC-3 tumor bearing mice

Organ, tissue and tumor uptake was examined by acute biodistribution studies of ^{64}Cu-DOTA-pHLIP after injection into male nude mice bearing either LNCaP or PC-3 tumors (Table 1). One additional group of PC-3 bearing mice received the equivalent mass of ^{64}Cu-DOTA-K-pHLIP as a control. The PC-3 tumor accumulation of ^{64}Cu-DOTA-pHLIP reached a maximum after 4 h (2.78 ± 0.19 %ID/g) and the tumor retention was high, with 2.46 ± 0.57 %ID/g remaining at 24 h. In the LNCaP mice, tumor accumulation of ^{64}Cu-DOTA-pHLIP reached a maximum after only 1 h (4.50 ± 1.71 %ID/g) and the tumor retention was also high, with 3.23 ± 0.55 %ID/g remaining at 24 h and 1.74 ± 1.41 %ID/g at 48 post-injection. The biodistribution data for ^{64}Cu-DOTA-pHLIP showed that the radioactive background in the blood and blood-rich organs, such as liver, lung, heart and spleen, were similar in the two tumor models while differences were noted in the tumors. Examination of tumor-to-tissue ratios (Figure 2) clearly shows that, for imaging purposes, the 4 h timepoint is optimal for both tumor models. This can be attributed to the better retention of the agent in tumor tissue and the more rapid washout of activity from background organs.

The administration of the mutant peptide, ^{64}Cu-DOTA-K-pHLIP, resulted in a ~40% lower PC-3 tumor accumulation at 1 h post-injection which is impressive in that the subsequent MRS study showed the PC-3 tumors to be less acidic. However, distribution of the control peptide, ^{64}Cu-DOTA-K-pHLIP, was similar in pattern to the parent, ^{64}Cu-DOTA-pHLIP, although with a reduction in accumulation in all tissues. The most likely reason for this universal reduction is a more rapid excretion of the mutant-pHLIP, which has been observed by fluorescence imaging as well, and, as a consequence, less retention in the blood and therefore the tissues. Our biophysical studies indicate that pHLIP binds to the surfaces of membranes at normal pH (26), which might lead to the slow kinetics of peptide distribution in vivo. Most probably, the mutant pHLIP has reduced binding affinity to the membrane, and, therefore, a faster kinetic profile. It is important to note that the mutant peptide was not taken up to the same extent by the skin or the kidney, which are tissues known to be more acidic than all other healthy tissues and organs.

The final groups of animals studied were LNCaP-bearing mice that were given either normal drinking water or water spiked with sodium bicarbonate to modulate the tumor pH_e. As shown by MRS, the bicarbonate water resulted in the modulated tumor having a more basic pH_e (*vide infra*). The results of the biodistribution in these mice (Table 2) were similar to those for LNCaP tumors presented in Table 1, but it is important to note that these studies were performed on

different dates with mice that had been implanted with a different passage of LNCaP cells. Except for uptake in the tumor and kidney, no significant differences were observed between the two groups in the 17 collected organs and tissues. ^{64}Cu-DOTA-pHLIP uptake in the non-modulated LnCAP tumors was *greater* than the uptake in the tumors in mice that received 7 days of bicarbonated water (4.50 ± 1.71 vs. 1.31 ± 0.60, respectively, $P = 0.005$).

Small Animal PET Imaging of ^{64}Cu-DOTA-pHLIP in PC3 and LNCaP prostate tumors

Delineation of the tumor by uptake of ^{64}Cu-DOTA-pHLIP was evident in both tumor models (Figure 3) but to a greater extent in the LNCaP bearing mice, while ^{64}Cu-DOTA-K-pHLIP did not exhibit any targeting ability (data not shown). In the PC-3 model, the tumor to muscle ratios derived from the SUV values for uptake of native peptide at 1, 4, and 24 hours were 1.45 ± 0.09, 2.67 ± 0.40, and 4.64 ± 1.08, showing a gradual increase in tumor uptake with concurrent washout from non-target organs. The tumor to muscle ratios derived from the SUV values in the LNCaP tumor model were significantly higher ($P = 0.0001$), with values of 3.44 ± 0.50, 5.56 ± 0.21 and 6.55 ± 1.98 for the 1, 4 and 24 hour time points, respectively.

MRS directly measures the volume-average pH_e of tumors

The acute biodistribution data and imaging results presented above demonstrate higher uptake and retention of ^{64}Cu-DOTA-pHLIP in the non-alkalinized LNCaP tumors, and suggest that the extracellular pH of LNCaP tumors is more acidic than that of PC-3 tumors. To determine tumor-average pH_e directly, ^{31}P MR spectroscopy measurements with the exogenous extracellular pH marker 3-APP were used (Figure 4). PC-3 and LNCaP tumor models were selected for pH measurements based on their significantly different SUV values as measured by PET, with LNCaP showing more uptake of the pHLIP peptide than PC-3. This difference was mirrored in the pH values determined by MR, with the LNCaP tumors showing a significantly more acidic average pH_e (6.78 ± 0.29) when compared to the PC-3 tumors (7.23 ± 0.10) ($P = 0.039$). Additional evidence that the ^{64}Cu-DOTA-pHLIP targeted pH_e was provided in the study in LNCaP tumors in which half of the mice were fed bicarbonated water prior to the biodistribution. As expected, in this experiment the average pH_e in the non-modulated LnCAP tumors was more acidic than the average pH_e of the tumors in mice having received 7 days of bicarbonated water (6.62 ± 0.35 vs. 6.94 ± 0.56, respectively $P = 0.28$). This correlates well with the data from the biodistribution where ^{64}Cu-DOTA-pHLIP uptake in the non-modulated LnCAP tumors was greater that the uptake in the tumors in mice having received 7 days of bicarbonated water (4.50 ± 1.71 vs. 1.31 ± 0.60, respectively, $P = 0.005$). It should also be noted that the pH_e measured in our MRS experiments is a volume-averaged pH_e. Although this measured pHe provides a good indication of the acidity outside of the cell, it may not reflect the exact pH on the exterior surface of the cells and does not account for tumor heterogeneity. Thus, pHe as measured by MRS is an indicator, but not a direct measure, of the pH causing insertion.

Discussion

The physiological differences between normal and tumor tissues provide an opportunity for the development of novel diagnostic and therapeutic agents specifically targeting cancer cells. However, the acidic extracellular environment in tumors has not been properly exploited, probably due to a lack of compounds whose properties change dramatically in the range of pH 6.0–7.5. The significance of the current work is that it proposes an innovative and novel method to target tumors based on an intrinsic physiological property - the acidic extracellular environment, and thereby addresses an important problem in the diagnosis and monitoring or response to therapy of cancer. The method is based on the pH-selective interaction of the pHLIP peptide with cell membranes. In this study, we have demonstrated and validated a novel, pH-

selective PET tracer - ^{64}Cu-DOTA-pHLIP. This is the first time a *peptide*-based PET agent has been employed for the delineation of the pH_e of tumors.

Our data show that ^{64}Cu-DOTA-pHLIP is stable in tumors. None of the animals in any of the studies showed any adverse effects due to the administration of any of the pHLIP constructs. The biodistribution and PET imaging data demonstrated retention of radioactivity in the tumors over 24 h. The tumor uptake of ^{64}Cu-DOTA-pHLIP correlates well with *in vivo* fluorescence imaging studies, which demonstrated that Cy5.5-pHLIP and Alexa750-pHLIP stayed in tumors for several (>4) days (25). This long retention might be explained by the fact that when the peptide is inserted into the cell membrane it is protected from attack by proteases, allowing it to accumulate in tumor tissue in significant amounts.

There are two main factors that might contribute to the accumulation of pHLIP peptides in non-tumor tissue. While at normal, physiological pH the probability of pHLIP insertion into the cell membrane is low, the peptide still interacts with the surface of the membrane through its hydrophobic motif. Although this produces a small background signal, it also allows for a longer blood circulation of pHLIP, enhancing the probability of delivering functional imaging moieties or therapeutic cargo to the site of disease. The background signal decreases with time, while the signal in tumors remains static or is enhanced. A second reason for unwanted background is the relative instability of the ^{64}Cu-DOTA chelation. ^{64}Cu has been shown to dissociate *in vivo* from DOTA and DOTA-conjugates, undergoing subsequent metabolism and trans-chelation to superoxide dismutase and other proteins, resulting in increased accumulation in the blood and liver (27,34,35). This could account, in part, for the main differences in biodistribution between Cy5-pHLIP and ^{64}Cu-DOTA-pHLIP, particularly the difference in liver uptake. In contrast to the PET results, the fluorescence data showed a very low uptake of Cy5.5-pHLIP by the liver (25), since the NIR dyes were conjugated covalently to the N-terminus of the peptide. We therefore believe that the apparent liver uptake of ^{64}Cu-DOTA-pHLIP could be significantly decreased by optimizing the copper-chelating moiety. The cross-bridged cyclam chelator, CBTE2A, has demonstrated improved *in vivo* stability and consequently a reduction in transchelation (35,36), but requires elevated temperatures for copper complexation that may not compatible with the pHLIP peptide construct.

The control peptide, ^{64}Cu-DOTA-K-pHLIP, which had just two amino acid residues replaced, demonstrated ~40% less PC-3 tumor uptake as early as 1 hour post-injection; we did anticipated that the mutant peptide would have lower uptake in the PC-3 model (the less acidic tumor) than the parent pHLIP. Also, small-animal PET imaging experiments showed that control peptide did not accumulate in tumors, consistent with previous fluorescence studies (25). Also we observed lowering of K-pHLIP level in blood and tissues, even though the equivalent mass of labeled K-pHLIP was administered and the data is normalized to the injected dose (%ID/g). We assume that rapid excretion of the mutant-pHLIP could be associated with its reduced affinity to the membrane at normal pH, in contrast to the parent pHLIP. Our thermodynamic studies indicated that pHLIP has high affinity to the membrane at normal pH ($\Delta G_{binding}$ is about −7 kcal/mol at 37°C) (26), which is probably associated with the prolongated peptide circulation in the blood. The pHLIP affinity to the cell membrane increases in an environment of low pH, at which point pHLIP inserts into the membrane and adopts a stable transmembrane configuration. In contrast to pHLIP, the mutant peptide K-pHLIP cannot insert into the cell membrane to form a transmembrane alpha-helix (25), so it can be assumed that the tumor uptake we observed for ^{64}Cu-DOTA-K-pHLIP in the acute biodistribution studies must be due to the passive diffusion of the construct into the tumor interstitium. Also, as stated, we cannot exclude the possibility that the creation of ^{64}Cu bound to serum proteins by exchange with ^{64}Cu-DOTA-pHLIP contributes to the background, especially at early time points. Therefore, even though it is known that K-pHLIP does not target acidity the use of K-pHLIP may not be an appropriate control system.

The selectivity of the pHLIP peptide was demonstrated by the modulation of pH_e in LNCaP-bearing mice in which more acidic LNCaP tumors had greater uptake of ^{64}Cu-DOTA-pHLIP than the less-acidic (bicarb-modulated) LNCaP tumors. As can be seen from Table 2, it is clear that administering sodium bicarbonate significantly altered the uptake of the peptide only in the tumor and kidney. Unlike with k-pHLIP (Table 1) there were no significant differences in the uptake by the skin, which cannot be explained at this time. The use of bicarbonate is known to have a profound effect on pH_e.(12,25,29) For example, Raghunand et al, showed with ^{31}P-magnetic resonance spectroscopy (MRS) that the pH_e of MCF-7 human breast cancer xenografts can be effectively and significantly raised with sodium bicarbonate in drinking water.(12) This was achieved with the mice drinking *ad libitum* water containing 200 mM $NaHCO_3$ for periods up to 90 days continuously, without any changes in subjective parameters and weight gain compared to control mice. In this current study the average pH_e in the non-modulated LnCaP tumors was more acidic than the average pH_e of the tumors in mice having received 7 days of bicarbonated water (6.62 ± 0.35 vs. 6.94 ± 0.56, respectively p = 0.28). This correlated well with the data from the acute biodistribution where ^{64}Cu-DOTA-pHLIP uptake in the non-modulated LnCaP tumors was significantly greater that the uptake in the tumors in mice having received 7 days of bicarbonated water (4.50 ± 1.71 vs. 1.31 ± 0.60, respectively, p = 0.005).

Apart from the liver and blood uptake, the quantitative PET data and images are in general agreement with the biodistribution studies and the previous reported fluorescence studies (25), including uptake of the peptide by the kidney. The kidney has acidic regions and is a major site of catabolism of low-molecular-weight proteins. The kidney uptake can be reduced by providing mice with bicarbonate-buffered drinking water at pH 8.0 (12,25,29), or drugs like acetozalomide, a carbonic anhydrase inhibitor that causes urinary alkalization. This reduction in kidney uptake with bicarbonate-buffered drinking water was confirmed in our own study presented in Table 2.

In summary, we have synthesized and evaluated the first generation of novel pH_e sensitive peptide PET agents for the delineation of low pHe in tumors. This is the first report of this novel class of PET imaging agents. Although the biokinetics of the agent are not optimal, additional strategies are currently under development to enhance tumor accumulation while reducing unwanted background uptake. This first generation agent offers the possibility of designing a new class of non-invasive pH-selective PET imaging agents that will be useful for the imaging of a broad range of disease states. Multimodal (diagnostic + therapeutic) pHLIP peptides with an N-terminus imaging label and C-terminus chemotherapeutic cargo (23) would afford the opportunity to monitor drug delivery, providing a key tool in efforts to predict therapeutic outcome.

Acknowledgments

The authors thank Dr. Artem Lebedev for his help as well as Chris Sherman, Amanda Roth, Nicole Fettig, Margaret Morris, Lori Strong and Susan Adams for technical support.

Financial Support: NIH R24 CA83060; P30 CA91842; DOD PC040435 to JSL; NIH R01 GM073857 to DME; NIH R01 133890 to OAA, DME and YRK; DOD PC050351 to YKR; DOD BC061356 and NIH R21 CA125280 to OAA; and the NIH for salary support of ALV F32 CA110422–03.

References

1. Bild AH, Potti A, Nevins JR. Linking oncogenic pathways with therapeutic opportunites. Nat Rev Cancer 2006;6:735–41. [PubMed: 16915294]
2. Cairns R, Papandreou I, Denko N. Overcoming physiologic barriers to cancer treatment by molecularly targeting the tumor microenvironment. Mol Cancer Res 2006;4:61–70. [PubMed: 16513837]

3. Coffey DS, Getzenberg RH, DeWeese TL. Hyperthermic biology and cancer therapies. JAMA 2006;296:445–8. [PubMed: 16868303]
4. Rofstad EK, Mathiesen B, Kindem K, Galappathi K. Acidic extracellular pH promotes experimental metastasis of human melanoma cells in athymic nude mice. Cancer Res 2006;66:6699–707. [PubMed: 16818644]
5. Stubbs M, McSheehy PM, Griffiths JR. Causes and consequences of acidic pH in tumors: a magnetic resonance study. Adv Enzyme Regul 1999;39:13–30. [PubMed: 10470364]
6. Gillies RJ. Causes and consequences of hypoxia and acidity in tumors. Trends Mol Med 2001;7:47–9. [PubMed: 11330256]
7. Raghunand N, Gillies RJ. pH and Chemotherapy. Novartis Fdn Symposium 2001;240:199–211.
8. Rajendran JG, Krohn KA. Imaging hypoxia and angiogenesis in tumors. Radiol Clin North Am 2005;43:169–87. [PubMed: 15693655]
9. Lora-Micheils M, Yu D, Sanders L, et al. Extracellular pH and P-31 magnetic resonance spectroscopic variables are related to outcome in canine soft tissue sarcomas treated with thermoradiotherapy. Clin Cancer Res 2006;12:5733–40. [PubMed: 17020978]
10. Gerweck LE, Vijayappa S, Kozin S. Tumor pH controls the *in vivo* efficacy of weak acid and base chemotherapeutics. Mol Cancer Therapeutics 2006;5:1275–9.
11. Raghunand N, Gillies RJ. pH and drug resistance in tumors. Drug Resistance Updates 2000;3:39–47. [PubMed: 11498364]
12. Raghunand N, He X, van Sluis R, et al. Enhancement of chemotherapy by manipulation of tumour pH. Br J Cancer 1999;80:1005–11. [PubMed: 10362108]
13. Garcia-Martin ML, Martinez GV, Raghunand N, Sherry AD, Zhang S, Gillies RJ. High resolution pH_e imaging of rat glioma using pH-dependent relaxivity. Magn Reson Med 2006;55:309–15. [PubMed: 16402385]
14. Bhujwalla ZM, Artemov D, Ballesteros P, Cerdan S, Gillies RJ, Solaiyappan M. Combined vascular and extracellular pH imaging of solid tumors. NMR Biomed 2002;15:114–9. [PubMed: 11870907]
15. Bhujwalla ZM, McCoy CL, Glickson JD, Gillies RJ, Stubbs M. Estimations of intra- and extracellular volume and pH by ^{31}P magnetic resonance spectroscopy: effect of therapy on RIF-1 tumours. Br J Cancer 1998;78:606–11. [PubMed: 9744499]
16. Garcia-Martin ML, Hérigault G, Rémy C, et al. Mapping extracellular pH in rat brain gliomas in vivo by 1H magnetic resonance spectroscopic imaging: comparison with maps of metabolites. Cancer Res 2001;61:6524–31. [PubMed: 11522650]
17. Gallagher FA, Kettunen MI, Day SE, et al. Magnetic resonance imaging of pH in vivo using hyperpolarized ^{13}C-labelled bicarbonate. Nature Med 2008;453:940–3.
18. Gillies RJ, Raghunand N, Karcamar GS, Bhujwalla ZM. MRI of the tumor microenvironment. J Magn Reson Imaging 2002;16:430–50. [PubMed: 12353258]
19. Blower PJ, Lewis JS, Zweit J. Copper radionuclides and radiopharmaceuticals in nuclear medicine. Nucl Med Biol 1996;23:957–80. [PubMed: 9004284]
20. Lewis JS, Welch MJ, Tang L. Workshop on the Production, application and clinical translation of ‘non-standard’ PET nuclides: a meeting report. Q J Nucl Med Molecular Imaging 2008;52:101–6.
21. Anderson CJ, Dehdashti F, Cutler PD, et al. Cu-64-TETA-Octreotide as a PET imaging agent for patients with neuroendocrine tumors. J Nucl Med 2001;42:213–21. [PubMed: 11216519]
22. Vavere AL, Lewis JS. Cu-ATSM: A radiopharmaceutical for the PET imaging of hypoxia. Dalton Trans 2007:4893–902. [PubMed: 17992274]
23. Reshetnyak YK, Andreev OA, Lehnert U, Engelman DM. Translocation of a molecules into cells by pH-dependent insertion of a transmembrane helix. Proc Natl Acad Sci USA 2006;103:6460–5. [PubMed: 16608910]
24. Reshetnyak YK, Segala M, Andreev OA, Engelman DM. A monomeric membrane peptide that lives in three worlds: in solution, attached to, and inserted across lipid bilayers. Biophys J 2007;93:2363–72. [PubMed: 17557792]
25. Andreev OA, Dupuy AD, Segala M, et al. Mechanism and uses of a membrane peptide that targets tumors and other acidic tissues *in vivo*. Proc Natl Acad Sci USA 2007;104:7893–8. [PubMed: 17483464]

26. Reshetnyak YK, Andreev OA, Segala M, Markin VS, Engelman DM. Energetics of peptide (pHLIP) binding to and folding across a lipid bilayer membrane. Proc Natl Acad Sci U S A 2008;105:15340–5. [PubMed: 18829441]
27. Wadas TJ, Wong EH, Weisman GR, Anderson CJ. Copper chelation chemistry and its role in copper radiopharmaceuticals. Curr Pharm Design 2007;13:3–16.
28. McCarthy DW, Shefer RE, Klinkowstein RE, et al. Efficient production of high specific activity ^{64}Cu using a biomedical cyclotron. Nucl Med Biol 1997;24:35–43. [PubMed: 9080473]
29. Evelhoch JL, Gillies RJ, Karczmar GS, et al. Applications of magnetic resonance in model systems: cancer therapeutics. Neoplasia 2000;2:152–65. [PubMed: 10933074]
30. Tai YC, Ruangma A, Rowland DJ, et al. Performance evaluation of the microPET Focus: A third-generation microPET scanner dedicated to animal imaging. J Nucl Med 2005;46:455–63. [PubMed: 15750159]
31. Gillies RJ, Liu Z, Bhujwalla Z. ^{31}P-MRS measurements of extracellular pH of tumors using 3-aminopropylphosphonate. Am J Physiol 1994;267:C195–C203. [PubMed: 8048479]
32. Bretthorst G. Bayesian analysis. III. Applications to NMR signal detection, model selection, and parameter estimation. J Magn Reson 1990;88:571–95.
33. Ackerman JJH, Soto GE, Spees WM, Zhu Z, Evelhoch JL. The NMR chemical shift pH measurement revisited: Analysis of error and modeling of a pH dependent reference. Magn Reson Med 1996;36:674–83. [PubMed: 8916017]
34. Boswell CA, Sun X, Niu W, et al. Comparative in vivo stability of copper-64-labeled cross-bridged and conventional tetraazamacrocyclic complexes. J Med Chem 2004;47:1465–74. [PubMed: 14998334]
35. Sprague JE, Peng Y, Sun X, et al. Preparation and biological evaluation of copper-64-labeled Tyr^3-octreotate using a cross-bridged macrocyclic chelator. Clin Cancer Res 2004;10:8674–82. [PubMed: 15623652]
36. Wei L, Butcher C, Miao Y, et al. Synthesis and biological evaluation of Cu-64 labeled rhenium-cyclized α-MSH peptide analog using a cross-bridged cyclam chelator. J Nucl Med 2007;48:64–72. [PubMed: 17204700]

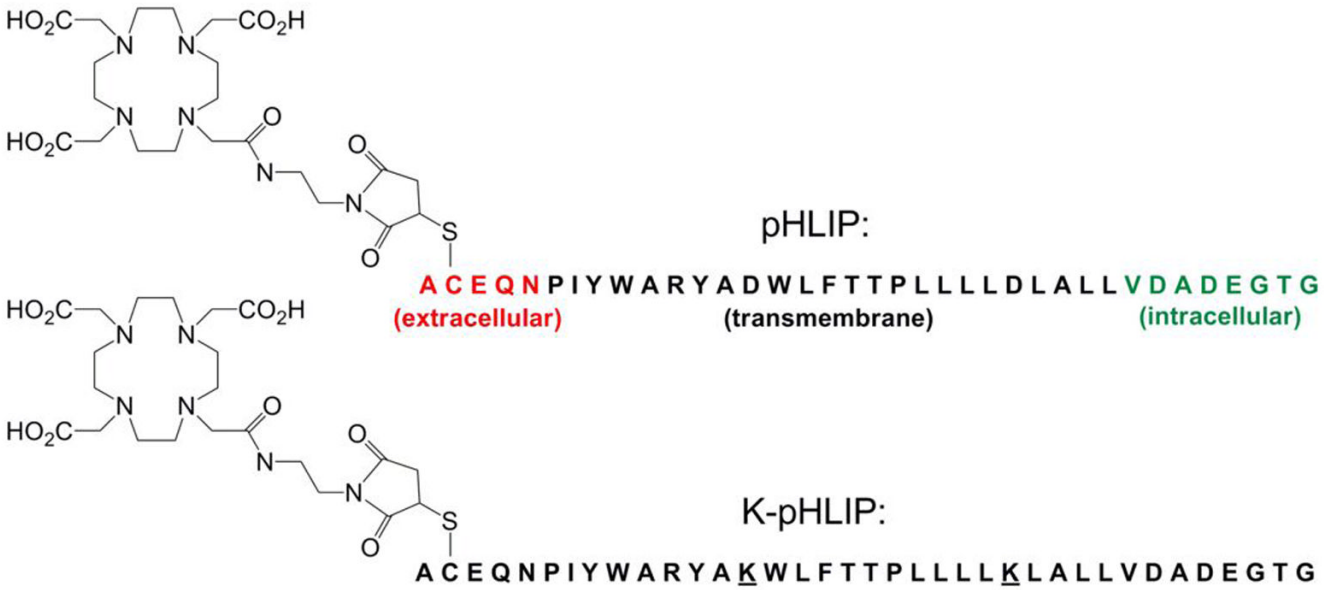

Figure 1.
Amino acid sequence of the native peptide compared to the mutant pHLIP (K-pHLIP).

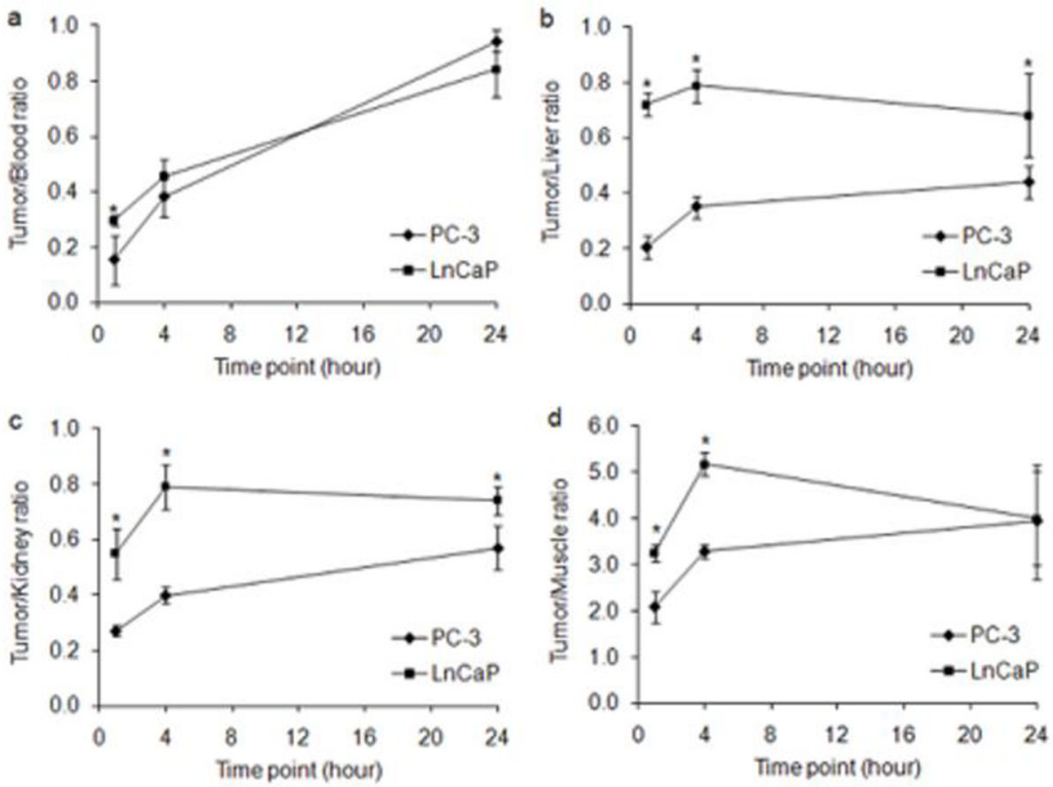

Figure 2.

Comparisons of various tumor-to-tissue ratios from ^{64}Cu-DOTA-pHLIP biodistribution data presented in Table 1. Tumor %ID/g was divided by the corresponding %ID/g of the tissue of interest for (a) blood (b) liver (c) kidney and (d) muscle. *Denotes statistical significance at the 95% confidence level ($P < 0.05$).

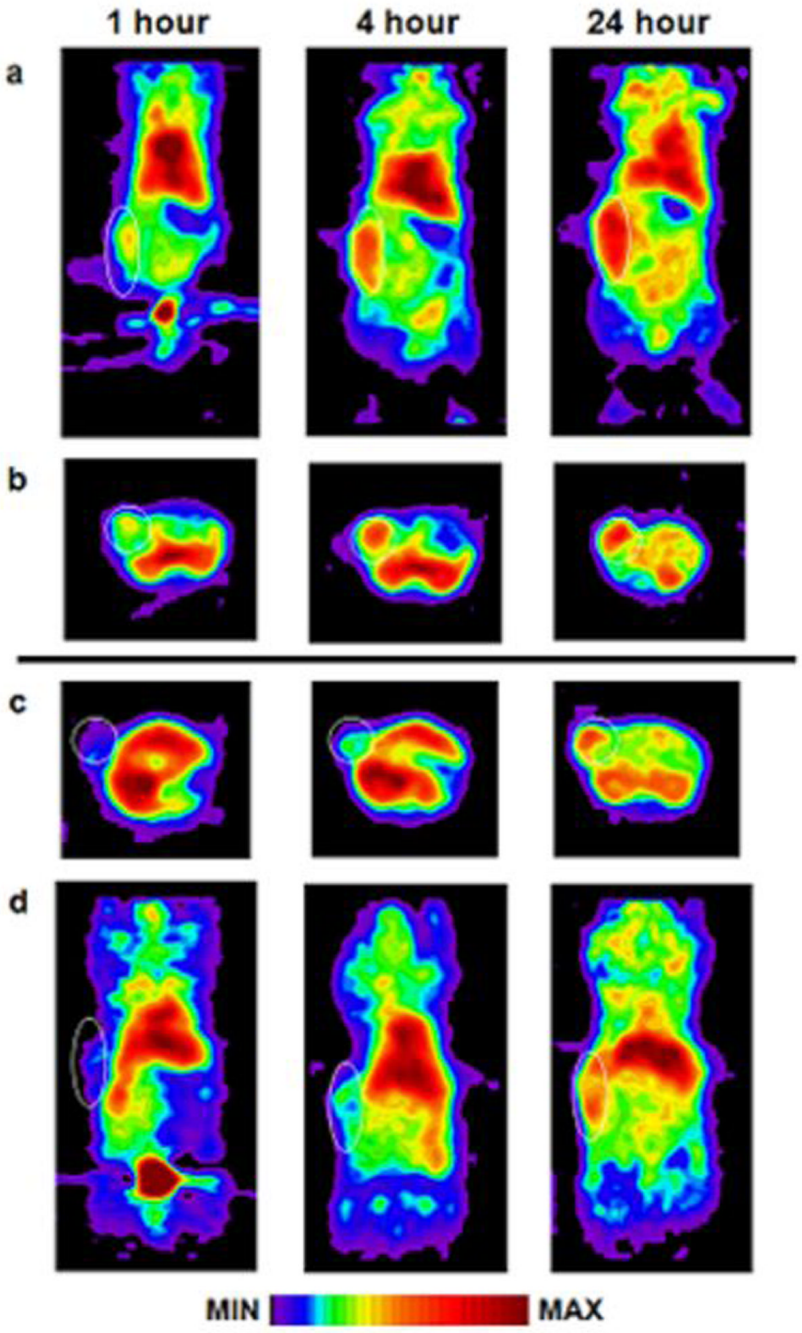

Figure 3.

Representative small-animal PET image slices of ^{64}Cu-DOTA-pHLIP (200 μCi per animal) in LNCaP (measured tumor $pH_e = 6.78 \pm 0.29$) and PC-3 (measured tumor $pH_e = 7.23 \pm 0.10$) tumor-bearing mice at various post- injection time points. Differences in tumor SUV values can be visualized by comparing the LNCaP (a) coronal and (b) transaxial slices to the PC-3 (c) transaxial and (d) coronal slices. In each image, the tumor is denoted by a white circle.

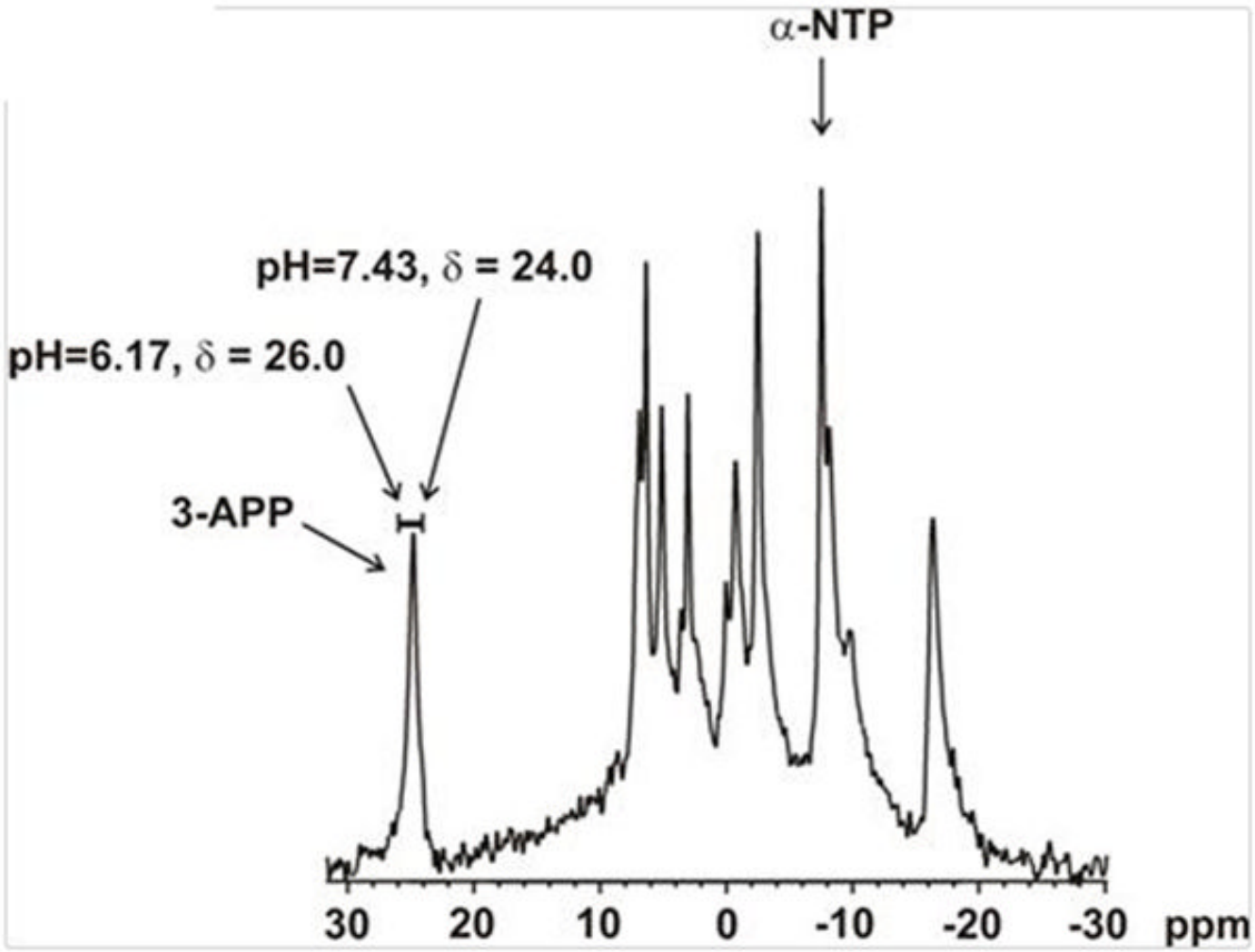

Figure 4. In vivo

^{31}P MR spectrum of a PC-3 tumor. Extracellular pH is estimated from the chemical shift difference (in ppm) between the extracellular pH indicator 3-APP and the pH-independent chemical shift of α-NTP. The scale bar above the 3-APP resonance indicates a range of chemical shifts (δ) from 24.0 to 26.0 ppm, corresponding to the physiologic range of pH_e (6.17 – 7.43).

Table 1

Acute biodistribution of ^{64}Cu-DOTA-pHLIP in tissues in PC-3 and LNCaP mice and ^{64}Cu-DOTA-K-pHLIP in PC-3 mice.

PC-3	1 hour Cu-64-DOTA-pHLIP	4 hour Cu-64-DOTA-pHLIP	24 hour Cu-64-DOTA-pHLIP	1 hour Cu-64-DOTA-K-pHLIP
blood	11.27 ± 0.81	7.45 ± 1.76	2.59 ± 0.48	7.09 ± 0.67
lung	5.16 ± 0.51	4.25 ± 0.94	2.35 ± 0.46	3.75 ± 0.18
liver	8.56 ± 1.14	7.99 ± 1.28	5.86 ± 1.23	5.21 ± 1.75
spleen	2.10 ± 0.14	2.02 ± 0.47	1.82 ± 0.44	1.64 ± 0.29
kidney	6.32 ± 0.39	6.93 ± 0.83	4.64 ± 1.27	4.63 ± 0.35*
muscle	1.11 ± 0.79	0.86 ± 0.16	0.65 ± 0.14	0.56 ± 0.09
skin	1.77 ± 0.09	2.07 ± 0.36	1.87 ± 0.33	0.96 ± 0.06
fat	0.80 ± 0.39	0.86 ± 0.27	0.53 ± 0.18	1.09 ± 0.80
heart	3.95 ± 0.60	3.17 ± 0.83	1.67 ± 0.14	2.50 ± 0.55
brain	0.47 ± 0.11	0.35 ± 0.12	0.16 ± 0.04	0.30 ± 0.06
bone	1.55 ± 0.19	1.17 ± 0.41	0.81 ± 0.14	1.12 ± 0.41
PC-3	1.72 ± 0.17	2.78 ± 0.19	2.46 ± 0.57	1.04 ± 0.15
LNCaP	**1 hour Cu-64-DOTA-pHLIP**	**4 hour Cu-64-DOTA-pHLIP**	**24 hour Cu-64-DOTA-pHLIP**	**48 hour Cu-64-DOTA-pHLIP**
blood	14.97 ± 1.11	8.08 ± 0.35	3.96 ± 1.11	1.68 ± 0.35
lung	5.63 ± 0.62	4.38 ± 0.39	3.22 ± 0.53	2.22 ± 0.70
liver	6.53 ± 1.02	4.80 ± 0.72	4.88 ± 0.98	4.43 ± 0.74
spleen	2.75 ± 0.48	2.05 ± 0.09	1.84 ± 0.27	1.41 ± 0.35
kidney	8.34 ± 0.66	5.42 ± 0.58	4.48 ± 1.08	2.76 ± 0.50
muscle	1.38 ± 0.53	0.72 ± 0.11	0.85 ± 0.25	0.49 ± 0.10
skin	4.16 ± 1.72	2.35 ± 0.15	2.87 ± 0.54	1.68 ± 0.20
fat	2.40 ± 0.73	0.87 ± 0.17	0.60 ± 0.16	0.26 ± 0.14
heart	5.31 ± 1.03	3.60 ± 0.28	2.02 ± 0.31	1.45 ± 0.08
brain	0.45 ± 0.06	0.29 ± 0.05	0.24 ± 0.05	0.16 ± 0.04
bone	3.77 ± 1.88	1.03 ± 0.10	1.00 ± 0.28	0.60 ± 0.10
LNCaP	4.50 ± 1.71	3.67 ± 0.56	3.23 ± 0.55	1.74 ± 1.41

* Due to a technical error an additional group of mice were used to produce this data. Data presented as the percent injected dose per gram of tissue ± standard deviation (%ID/g ± SD) in n = 4–5 mice per group.

Table 2

Acute biodistribution in LNCaP-bearing mice split into two groups, (1) mice received 150 mM bicarbonated water at pH 8.0 ad libitum for 7 days prior the study, and (2) mice were fed regular drinking water. Data presented as the percent injected dose per gram of tissue ± standard deviation (%ID/g ± SD) in n = 4 mice per group.

	4 hour (untreated)	4 hour (modulated)
blood	7.21 ± 1.39	7.27 ± 1.00
lung	3.63 ± 0.63	3.85 ± 0.61
liver	5.29 ± 1.64	5.79 ± 0.66
spleen	1.49 ± 0.32	1.53 ± 0.25
kidney*	5.20 ± 1.06	3.78 ± 0.29
muscle	0.69 ± 0.40	1.05 ± 0.80
skin	1.12 ± 0.29	1.02 ± 0.27
fat	1.26 ± 1.42	1.16 ± 0.50
heart	2.07 ± 0.28	2.39 ± 0.44
brain	0.59 ± 0.69	0.27 ± 0.06
bone	1.22 ± 1.15	2.22 ± 2.51
pancreas	1.48 ± 0.77	1.56 ± 0.67
stomach	0.88 ± 0.58	1.01 ± 0.26
small int	2.05 ± 1.04	2.48 ± 0.59
upper lg int	2.35 ± 1.25	3.55 ± 1.94
lower lg int	1.28 ± 0.79	1.23 ± 0.54
LNCaP*	4.50 ± 1.71	1.31 ± 0.60

* Denotes statistical significance ($P < 0.005$) between the treated and non-treated groups. (lg int = large intestine)